

# Spontaneous emission from excitons in cylindrical dielectric waveguides and the spontaneous-emission factor of microcavity ring lasers

Daniel Y. Chu and Seng-Tiong Ho

*Department of Electrical Engineering and Computer Science, The Robert R. McCormick School of Engineering and Applied Science, The Technological Institute, Northwestern University, Evanston, Illinois 60208*

Received May 1, 1992; revised manuscript received August 21, 1992

The modification of the spontaneous emission from various dipoles in a cylindrical dielectric waveguide is studied as a function of the refractive index and the radius of the waveguide. It is found that the emission rates of the axial dipoles and the radial dipoles can be modified to enhance greatly the fraction of radial dipole emission that goes into the guided lasing modes. The total emission from the axial dipoles can be suppressed. This combination gives a high spontaneous-emission factor  $\beta$  for a microcavity ring laser. Other microlaser structures that have high  $\beta$  values are also discussed. We conclude that microlasers based on strongly guided single-mode dielectric waveguides are promising devices for achieving high  $\beta$  values and low lasing thresholds.

## 1. INTRODUCTION

Recently there has been much interest in the use of microcavities or dielectric structures to modify the rate or spatial pattern of spontaneous emission. It has been suggested that controlling spontaneous emission can reduce the laser threshold to very low (near-zero) levels.<sup>1-3</sup> Furthermore, nonclassical-number-state light and ultrahigh-speed (terahertz) modulation rates are predicted for such lasers.<sup>3</sup> Various methods have been proposed for modifying the spontaneous-emission rates. These methods include various types of microcavity and periodic dielectric structures with photonic band gaps. Several authors have reported the use of microcavities to modify spontaneous decay rates and to achieve near-zero threshold lasing theoretically and experimentally.<sup>4-18</sup> With photonic band gaps, as was first suggested by Yablonoitch,<sup>2,19</sup> huge reductions in the decay rates can be expected. The amount of reduction that can be achieved with photonic band gaps may be greater than that possible with microcavities.

The realization of near-zero threshold lasers, however, does not necessarily require that the net spontaneous decay rate be modified. It has been shown that there are two main factors that affect the laser threshold, namely, the transparency-current factor and the spontaneous-emission factor  $\beta$ .<sup>3,20,21</sup> The transparency current is the current at which the active medium becomes transparent, which is a necessary condition for lasing. The spontaneous-emission factor  $\beta$  is defined to be the rate of spontaneous emission into the lasing mode divided by the total rate of spontaneous emission.<sup>3,20,22</sup> Because of the relation between gain and spontaneous emission, an increase in spontaneous emission into the lasing mode means an increase in gain also. Hence, the larger the value for  $\beta$ , the less current is required above the trans-

parency current for lasing to occur. Thus, when the transparency current is small, increasing the  $\beta$  value toward unity will drastically reduce the laser threshold. The  $\beta$  value can be increased with an appropriate cavity design. For improvement in the value of  $\beta$  it is the spatial pattern of spontaneous emission that matters, not the change in the overall decay rate. For  $\beta = 1$  to be achieved, all the spontaneous emission must be into the lasing mode both spatially and spectrally. Spatially one wants an emission pattern that emits solely into the lasing mode. Spectrally one wants the spontaneous emission to couple into only one cavity resonance. The reduction of the overall decay rate, however, can be useful in reducing the amount of pumping that is necessary to achieve population inversion, as is apparent in a three-level laser model. Hence decay-rate reduction can be used to reduce the transparency current.

In this paper our focus is on the modification of the  $\beta$  value. The  $\beta$  values for microcavities with plane dielectric mirrors were studied by Bjork *et al.*<sup>9</sup> and Baba *et al.*<sup>22</sup> Here we analyze the case of a ring cavity in which the lasing mode is guided along a ring dielectric waveguide. Such a microring laser could be realized with microelectronic techniques that are similar to those used for creating microdisk lasers and microcavities.<sup>16,17</sup> To treat this case, we first analyze the modification of spontaneous emission when a dipole is placed at the axis of a cylindrical dielectric waveguide. The analysis is given in Section 3. In Section 4 we consider an example that may be realized with semiconductor materials. We study the modification of the spontaneous emission from the dipoles as a function of the waveguide diameter for this example. In Section 5 we consider the extreme cases in which the waveguide diameter approaches zero and infinity. In Sections 6 and 7 we estimate the spontaneous-emission factor  $\beta$  for microring lasers. We discuss both an ideal

ring structure with an optimal  $\beta$  value and a more practical structure. We also apply our result to the case of a vertical-cavity laser with vertical waveguiding.

## 2. WAVEGUIDE STRUCTURE OF INTEREST

We analyze the spontaneous emission from excitons at the center axis of a cylindrical dielectric waveguide. The excitons can be the excited carriers in a quantum wire that is located along the waveguide axis. The excitons will be modeled as three independent dipoles. One of the dipoles is parallel to the waveguide axis and is referred to as the axial dipole. The other two dipoles are perpendicular to the waveguide axis and are referred to as the radial dipoles. The dielectric waveguide structure is shown in Fig. 1. It is a step-index cylindrical waveguide with diameter  $d_D$ , where the high-index core region has refractive index  $n_D$  and the surrounding cladding region has refractive index  $n$ . For example,  $n_D$  can be the refractive index of AlGaAs or InP, with a value of approximately 3–3.5, and  $n$  can be the refractive index of air ( $n = 1$ ). The refractive index of the active center region that is occupied by the dipoles is assumed to be the same as or close to  $n_D$ . It is also assumed that the diameter of the active region,  $d_A$ , is small compared with one optical wavelength,  $\lambda/n_D$ , where  $\lambda$  is the exciton emission wavelength in free space.

In our calculation the spontaneous decay is modeled as stimulated decay arising from stochastic vacuum-field fluctuation.<sup>9,23</sup> The dipoles interact with the vacuum-field modes from all directions. Let us denote the  $k$  vector of any vacuum-field mode at the location of the dipoles by the spherical coordinates  $\theta_s$ ,  $\phi_s$ , and  $r_s$ , where  $\theta_s$  is the angle between the  $k$  vector of the field mode and the axis of the waveguide, which we define as the  $z$  axis (see Fig. 1). We use  $r$  to denote the radial distance from the axis of the cylindrical waveguide, so that the dipoles are at  $r = 0$  and the surface of the cylindrical waveguide is at  $r = d_D/2$ . Depending on the angle  $\theta_s$ , the vacuum-field modes at the dipoles can come from either the incident vacuum-field modes in the cladding index  $n$  (solid slanted line in Fig. 1) or the guided vacuum-field modes along the cylindrical waveguide (dashed zigzag in Fig. 1). When the vacuum-field modes in the index- $n$  cladding propagate into the waveguide, they become the vacuum field modes in the shaded region of Fig. 1. This shaded region is defined by the region within the critical angle for total internal reflection. We refer to these modes as the radiation modes for convenience. For each  $k$  vector there are two modes, corresponding to two polarizations. These are the TE and TM modes, as shown in Fig. 1, where the polarizations of the TE and TM modes are along the unit vector of  $\phi_s$  and  $\theta_s$ , respectively. The modes are labeled  $E_{\phi_s}$  and  $E_{\theta_s}$ .

Let us decompose the field around the dipoles in the dielectric into two components,  $E_{\phi_s}$  and  $E_{\theta_s}$ . We note that  $E_{\phi_s}$  is tangential to the dielectric surface of the wire and has no component along the  $z$  axis, while  $E_{\theta_s}$  has components parallel and perpendicular to the  $z$  axis. Since only  $E_{\theta_s}$  has a component parallel to the  $z$  axis, the axial dipole radiates solely into  $E_{\theta_s}$ . Similar arguments indicate that the radial dipoles radiate into both  $E_{\theta_s}$  and  $E_{\phi_s}$ . The main part of our decay-rate calculation is to find the vacuum-

field strengths of  $E_{\theta_s}$  and  $E_{\phi_s}$  of the various vacuum-field modes around the dipoles. From the vacuum-field strength the decay rates of the dipoles can then be obtained.

## 3. DECAY-RATES CALCULATION

We denote the dipole moment operator for an excited dipole under consideration as  $\hat{\mathbf{d}}$ . To calculate the net decay rate for a dipole  $\hat{\mathbf{d}}$ , we first compute the incremental contribution to the decay rate from the vacuum-field modes at a particular direction  $\Omega = \{\theta_s, \phi_s\}$  and those lying within a small angle  $d\Omega$  of that direction. Let us denote this incremented contribution by  $d\gamma(\Omega)$ . The standard decay-rate calculation, such as that given in Ref. 24, gives

$$d\gamma(\Omega) = (2\pi/\hbar^2) |\langle F | \hat{H}_{\text{int}} | I \rangle|^2 d\rho_F, \quad (3.1)$$

where  $\hat{H}_{\text{int}} = \hat{\mathbf{E}}_m \cdot \hat{\mathbf{d}}$ , with  $\hat{\mathbf{E}}_m$  being the macroscopic electric-field operator for a quantized mode propagating in that direction and where  $d\rho_F$  is the number of states per unit angular frequency within the solid angle  $d\Omega$ . The frequency of mode  $\mathbf{E}_m$  is at the resonant frequency of the dipole. A familiar example for  $\hat{\mathbf{E}}_m$  and  $d\rho_F$  is the case of free space, for which one has

$$d\rho_F = [V_Q/(2\pi)^3] k^2 (dk/d\omega) \sin(\theta_s) d\theta_s d\phi_s, \\ \hat{\mathbf{E}}_m = i\xi_m \mathbf{e}_m \hat{a}_m \exp(i\mathbf{k}_m \cdot \mathbf{r}) + \text{H.c.},$$

where H.c. denotes the Hermitian conjugate,  $\mathbf{e}_m$  is the polarization vector, and  $\xi_m = (\hbar\omega_A/2\epsilon_0 V_Q)^{1/2}$ . ( $\omega_A$  is the resonant frequency of the dipole.) Below we need to find the mode amplitude  $\xi_m$  for different cases. This mode amplitude can be found by requiring that the vacuum expectation value of the total mode energy be  $1/2\hbar\omega_A$ . That is,

$$\frac{1}{2} \int_{V_Q} d\mathbf{r} \langle 0 | (\epsilon \hat{\mathbf{E}}_m^2 + \mu_0 \hat{\mathbf{H}}_m^2) | 0 \rangle = \int_{V_Q} d\mathbf{r} \langle 0 | \epsilon \hat{\mathbf{E}}_m^2 | 0 \rangle = \frac{1}{2} \hbar\omega_A. \quad (3.2)$$

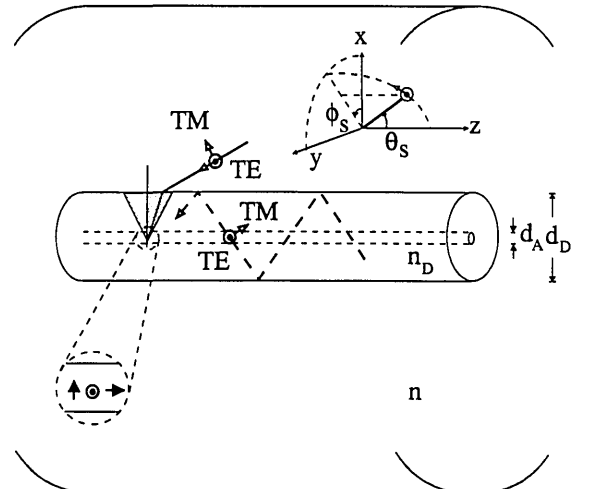


Fig. 1. Schematic of the cylindrical dielectric waveguide structure. The rays of a guided mode and a radiation mode are shown as the dashed zigzag and the solid slanted lines, respectively. The spherical coordinates are also indicated.

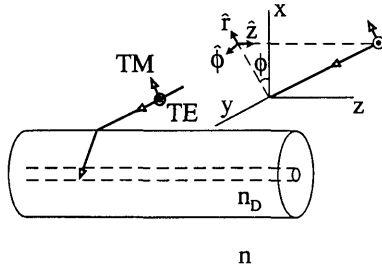


Fig. 2. Cylindrical coordinates used in the calculations.

For the cylindrical waveguide structure the contribution to the decay rate can be split into two parts, namely, that arising from the vacuum field in the guided modes  $\gamma_g$  and that arising from the vacuum field in the radiation mode  $\gamma_R$ . If the net decay rate is  $\gamma_{sp}$ , then  $\gamma_{sp} = \gamma_g + \gamma_R$ . Let us first calculate  $\gamma_g$ .

Let us consider a guided mode  $m$ . The macroscopic electric-field operator for the guided mode can be written as

$$\hat{\mathbf{E}}_m(r, \phi, z) = iA\mathbf{F}_m(r, \phi)\hat{a}_m \exp(ik_{mz}z) + \text{H.c.}, \quad (3.3)$$

where  $k_{mz}$  is the  $k$  vector in the  $z$  direction. The function  $\mathbf{F}_m(r, \phi)$  is the mode function for the guided mode. These guided modes are more conveniently expressed in terms of cylindrical coordinates instead of spherical coordinates. The cylindrical coordinates will be denoted by  $r, \phi$ , and  $z$  as shown in Fig. 2. The constant  $A$  in Eq. (3.3) is to be chosen so that Eq. (3.2) can be satisfied, as follows:

$$\frac{\hbar\omega_A}{2} = \int_0^{L_z} dz \int_{-\infty}^{\infty} dr \int_0^{2\pi} d\phi r \epsilon_r |\langle 0|\hat{\mathbf{E}}_m(r, \phi, z)|0\rangle|^2, \quad (3.4)$$

where

$$|\langle 0|\hat{\mathbf{E}}_m|0\rangle|^2 = |\mathbf{F}_m(r, \phi)|^2 A^2 \quad (3.5)$$

and  $\epsilon_r$  is the dielectric constant at  $r$ . This gives us

$$A^2 = \hbar\omega_A / (2L_z S), \quad (3.6)$$

where

$$S = \int_{-\infty}^{\infty} dr \int_0^{2\pi} d\phi r \epsilon_r |\mathbf{F}_m(r, \phi)|^2. \quad (3.7)$$

We note that the vacuum-field intensity at the dipole is proportional to  $A^2|\mathbf{F}_m|^2$  evaluated at the dipole. From Eqs. (3.6) and (3.7) we see that the intensity is inversely proportional to  $S$ , which is basically the transverse spatial area of the field mode times  $\epsilon_r$ . Thus we see that the larger the mode spatial area, the smaller the vacuum field intensity at the dipole. This is because the total energy of the mode must be equal to  $\hbar\omega$ . The decay-rate contribution to  $\gamma_g$  from mode  $m$  will be denoted by  $\gamma_{gm}$ . Following Eq. (3.1),  $\gamma_{gm}$  is given by

$$\gamma_{gm} = \frac{2\pi}{\hbar^2} A^2 |\mathbf{F}_m \cdot \boldsymbol{\mu}|^2 \left( \frac{L_z}{2\pi} \right) \frac{dk_{mz}}{d\omega} \quad (3.8)$$

$$= \frac{2\pi}{\hbar^2} \frac{\hbar\omega_A}{2L_z S} |\mathbf{F}_m \cdot \boldsymbol{\mu}|^2 \left( \frac{L_z}{2\pi} \right) \frac{dk_{mz}}{d\omega}, \quad (3.9)$$

where  $\boldsymbol{\mu} = \langle u|\hat{\mathbf{d}}|g\rangle$  is the usual dipole moment matrix element between the excited and the ground states of the dipole atom. We have quantized the field in the  $z$  direction by means of the traveling-wave modes (with the period boundary condition within length  $L_z$ ) and the  $r$  direction by means of the waveguide modes. Thus the number of states per unit angular frequency is  $d\rho_F = [L_z/(2\pi)](dk_{mz}/d\omega)$  for each waveguide mode owing to the quantization of  $k_{mz}$ . Examples of the mode functions  $\mathbf{F}_m$  are discussed in Appendix A. The total decay rate  $\gamma_g$  is the sum of the rates for each guided mode  $\gamma_{gm}$ ,

$$\gamma_g = \sum_m \gamma_{gm}. \quad (3.10)$$

Next let us calculate the values for  $\gamma_R$ . Similar to the free-space case, the field mode at the dipole is taken as  $\hat{\mathbf{E}}_m = i\xi_m \mathbf{e}_m \hat{a}_m \exp(i\mathbf{k}_m \cdot \mathbf{r}) + \text{H.c.}$ . The incremental contribution to  $\gamma_R$  from the radiation modes at the dipole around the angle  $\Omega$  is given by

$$d\gamma_R(\Omega) = (2\pi/\hbar^2) |\xi_m|^2 |\mathbf{e}_m \cdot \boldsymbol{\mu}|^2 \rho_s \sin(\theta_s) d\theta_s d\phi_s, \quad (3.11)$$

where the spherical coordinates  $\theta_s$  and  $\phi_s$  are used. In Eq. (3.11),  $\rho_s \sin(\theta_s) d\theta_s d\phi_s$  is the density-of-states factor  $d\rho_F$  and  $\xi_m$  is the vacuum-field amplitude at the location of the dipoles. However, as every mode  $\xi_m$  in the structure actually comes from a quantized mode in the cladding medium of index  $n$ , we can relate each  $\xi_m$  to an incident vacuum mode in  $n$ , which will be denoted as  $\xi_m^{\text{cl}}$ . We know that a quantized mode in the  $n$  cladding has the amplitude  $\xi_m^{\text{cl}} = (\hbar\omega_A/2\epsilon V_Q)^{1/2}$  ( $\epsilon = \epsilon_0 n^2$ ). We can propagate mode  $\xi_m^{\text{cl}}$  into the structure and find its amplitude at the dipoles. Let us define  $G_m$  as the ratio  $G_m = \xi_m/\xi_m^{\text{cl}}$ . We can rewrite Eq. (3.11) in terms of incident modes in the cladding region and sum over all the incident modes, resulting in a net contribution to the decay rate that is given by

$$\gamma_R = 2 \int_0^{2\pi} d\phi_{\text{cl}} \int_0^{\pi/2} d\theta_{\text{cl}} \frac{2\pi}{\hbar^2} |\xi_m^{\text{cl}}|^2 |G_m|^2 |\mathbf{e}_m' \cdot \boldsymbol{\mu}|^2 \rho_{\text{cl}}(\sin \theta_{\text{cl}}), \quad (3.12)$$

where  $\mathbf{e}_m'$  is the polarization vector of that mode in the core region,  $\theta_{\text{cl}}$  is the incident angle in the cladding region,  $\rho_{\text{cl}} = [V_Q/(2\pi)^3] k^2 (dk/d\omega)$ ,  $k = \omega_A n/c$ , and  $dk/d\omega = n/c$ . We note that, for the case of an axial dipole that is coupled to the TM modes,  $|\mathbf{e}_m' \cdot \boldsymbol{\mu}|^2 = |\boldsymbol{\mu}|^2 (\sin^2 \theta_m)$ ; for the case of a radial dipole coupled to the TM modes,  $|\mathbf{e}_m' \cdot \boldsymbol{\mu}|^2 = |\boldsymbol{\mu}|^2 (\cos^2 \theta_m) (\sin^2 \phi_m)$ ; and, for the case of a radial dipole coupled to the TE modes,  $|\mathbf{e}_m' \cdot \boldsymbol{\mu}|^2 = |\boldsymbol{\mu}|^2 (\sin^2 \phi_m)$ . The axial dipole does not couple to the TE modes, because the dipole is perpendicular to the electric field in that case.

The factor  $G_m$  is not easy to calculate, because the modes in the waveguide experience reflections at the waveguide surface owing to the refractive-index step. As a result the modes, on entering the core, see a Fabry-Perot resonator with two parallel cylindrical mirrors formed by the waveguide surface. To simplify the problem we approximate the curved surface of the cylinder by flat surface. That is, the wave in the waveguide is assumed to bounce from a plane dielectric interface at the waveguide surface. As is discussed below, this approximation gives the correct numerical results when the

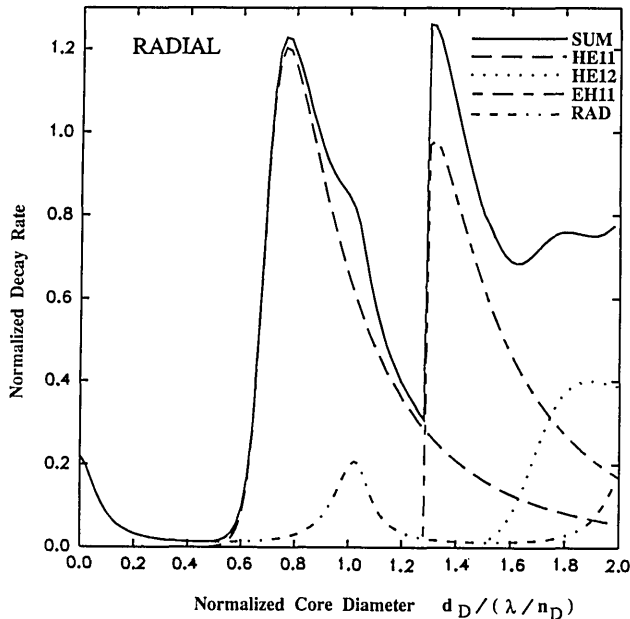


Fig. 3. Normalized decay rates  $R_g(\text{HE}_{11})$  ( $\text{HE}_{11}$ ),  $R_g(\text{HE}_{12})$  ( $\text{HE}_{12}$ ),  $R_g(\text{EH}_{11})$  ( $\text{EH}_{11}$ ), and  $R_R$  ( $\text{RAD}$ ) of the radial dipole versus the normalized core diameter. The total normalized decay rate  $R_{\text{sp}}$  ( $\text{SUM}$ ) of the radial dipole is also given (solid curve).

waveguide diameter  $d_D$  approaches zero. The approximation, however, does not give the correct quantitative result when  $d_D$  is large. Nevertheless, the approximation will at least tell us the qualitative behavior in the region of finite  $d_D$ . With this approximation  $G_m$  can be found with use of the transfer-matrix method,<sup>25</sup> yielding

$$G_m = \frac{(R_{21}/T_{21})\exp(ik_{mz}d_D/2)}{R_{21}(T_{21}T_{12} - R_{21}R_{12}/T_{12})\exp(ik_{mz}d_D) + (R_{12}/T_{12}T_{21})\exp(-ik_{mz}d_D)}, \quad (3.13)$$

where  $k_{mz} = 2\pi(\cos\theta_s)/(\lambda/n_D)$ ,  $\lambda = 2\pi c/\omega_A$ ,  $R_{21} = (h-g)/(g+h) = -R_{12}$ , and  $T_{21} = 2h/(g+h) = T_{12}g/h$ . Depending on the mode polarizations,  $g$  and  $h$  are given by  $g = 2\pi n(\cos\theta_{c1})$  [ $\text{TE}$ ] =  $2\pi(\cos\theta_{c1})/n$  [ $\text{TM}$ ] and  $h = 2\pi n_D(\cos\theta_s)$  [ $\text{TE}$ ] =  $2\pi(\cos\theta_s)/n_D$  [ $\text{TM}$ ]. The angles  $\theta_{c1}$  and  $\theta_s$  are related simply by the Snell's law of refraction. We have labeled the cladding as region 1 and the core as region 2. This gives us the label for the various  $R$  and  $T$  coefficients, so that  $R_{12}$ , for example, is the field reflection coefficient for the wave in the cladding as the wave goes into the core.

#### 4. RESULTS WITH SEMICONDUCTOR WAVEGUIDES

Examples of the decay rates for the radial and the axial dipoles are given in Figs. 3 and 4, respectively. In these examples we have taken  $n_D = 3.4$  and  $n = 1.0$ , which can be achieved with semiconductor materials as the cylindrical waveguide. The results are used below to discuss the spontaneous-emission factor for various semiconductor microcavity lasers. The core diameter ( $x$  axis in Figs. 3 and 4) is normalized by the optical wavelength  $\lambda/n_D$ . In the figures the curves represent the various contributions to the decay rates from the radiation modes or from the various guided modes. The rates are normalized so that the total emission rate for a dipole in the core has the

value unity when the core becomes a bulk medium in the limit of large core diameter. Let  $\gamma_\infty$  be the total decay rate of the horizontal or vertical dipole in a bulk medium of refractive index  $n_D$ . (The dipoles have the same rate in a bulk medium.) The various rates shown in the figures are the actual decay rates divided by  $\gamma_\infty$ . The normalized rates are labeled as  $R_R$  for radiation modes,  $R_g(m)$  for the various guided modes, and  $R_{\text{sp}}$  for the total rates [ $R_{\text{sp}} = R_R + \sum_m R_g(m)$ ]. In Fig. 3 the emission rate into the  $\text{HE}_{11}$  mode  $R_g(\text{HE}_{11})$  is given as the long-dashed curve, into the  $\text{HE}_{12}$  mode  $R_g(\text{HE}_{12})$  as the dotted curve, into the  $\text{EH}_{11}$  mode  $R_g(\text{EH}_{11})$  as the short-and-long-dashed curve, and into the radiation modes  $R_R$  as the three-dashed-two-dotted curve. In Fig. 4 the emission rate into the  $\text{TM}_{01}$  mode  $R_g(\text{TM}_{01})$  is given as the dashed curve and that into the radiation mode  $R_R$  as the dotted curve. The total decay rate  $R_{\text{sp}}$  is given as the solid curve for both dipoles. From the above calculations it is clear that the values of the decay rates are dependent on the values of both the density-of-states factor,  $dk_{mz}/d\omega$ , and the mode spatial area,  $S$ . The density-of-states factor,  $dk_{mz}/d\omega$ , is plotted in Fig. 5 as a function of the normalized core diameter for the dominant  $\text{HE}_{11}$  mode. We note the similarity between the leading edge of Fig. 5 and the leading edge of the decay-rate curve of the  $\text{HE}_{11}$  mode in Fig. 3. This behavior also holds for other modes. Hence we see that the leading-edge locations of the various modes in Figs. 3 and 4 are due mainly to the density-of-states factor instead of to the mode spatial area. We note that the number of guided modes is actually greater than that shown in Figs. 3 and 4. The missing modes do not show up in the figures owing to their lack of coupling to the dipoles. For

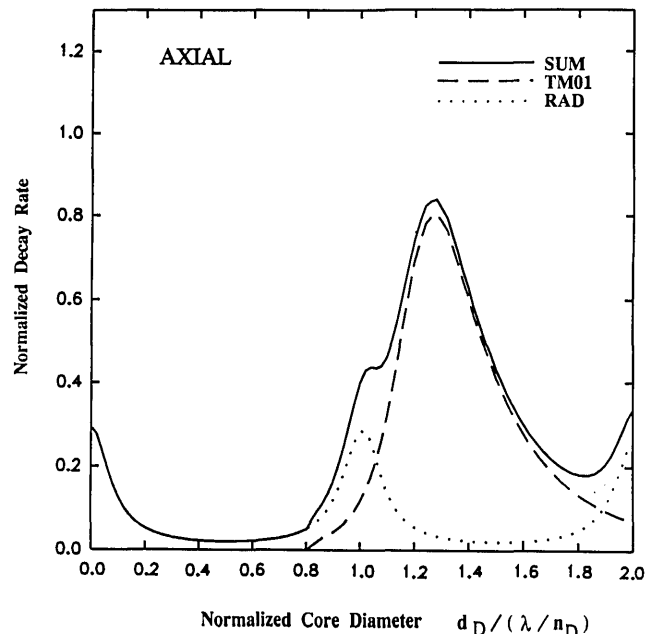


Fig. 4. Normalized decay rates  $R_g(\text{TM}_{01})$  ( $\text{TM}_{01}$ ) and  $R_R$  ( $\text{RAD}$ ) of the axial dipole versus the normalized core diameter. The total normalized decay rate  $R_{\text{sp}}$  ( $\text{SUM}$ ) of the axial dipole is also given (solid curve).

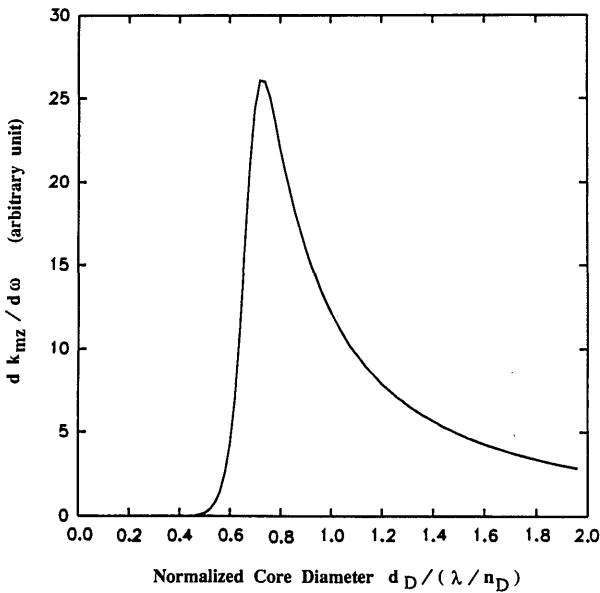


Fig. 5. Density-of-states factor,  $dk_{mz}/d\omega$ , versus the normalized core diameter for the  $HE_{11}$  mode.

example, for the  $TE_{01}$  mode  $F_r$  and  $F_z$  are zero everywhere, and  $F_\phi$  is vanishing at the dipoles. As a result there is no spontaneous decay into the  $TE_{01}$  mode.

## 5. DISCUSSION OF EXTREME CASES

In this section we consider two limiting cases, namely, the case in which the core diameter approaches zero and the case in which the core diameter is large. For the case in which the core diameter approaches zero we discuss the limiting values for the total spontaneous-emission rates, which can be derived by using simple physical arguments. This derivation allows us to verify our numerical calculation in that limit. For the case in which the core diameter is large we focus on the behavior of the radiation modes, which is relevant to the estimation of the spontaneous-emission factor for microcavity lasers.

In the limit when the wire diameter  $d_D$  is small compared with the optical wavelength, the coupling of the dipole to the guided modes vanishes. This is because the mode spatial area  $S$  must become infinitely large in that limit, and the vacuum-field intensity of the guided modes will be negligible at the dipoles. Hence the dipoles will couple only to the radiation modes. In this limit the field in the wire will become uniform. This means that the field at the dipole is equal to the field just below the wire surface. Also, it turns out that when the wire diameter is small the wire behaves as an on-resonant parallel-plate Fabry-Perot resonator with equal mirror reflectivities. As a result, any field that impinges upon the thin wire is totally transmitted through the wire without reflection. Furthermore, the net field just below the wire surface is related to the net field just above the surface by means of dielectric boundary conditions. Hence the net field at the dipole is just related to the impinging vacuum field by means of the dielectric boundary conditions. Specifically, the component of the field that is tangential to the boundary is continuous across the boundary, while the component of the field that is perpendicular to the boundary is attenuated by a factor of  $(n/n_D)^2$  when it enters the wire.

Let us call the vacuum-field components that are tangential and perpendicular to the wire surface the tangential and the perpendicular vacuum fields, respectively. This means that the tangential vacuum field in the wire will have a value that is the same as the vacuum field in the medium of index  $n$ . Similarly, the perpendicular vacuum field in the wire will be attenuated by a factor of  $(n/n_D)^2$  from the vacuum field in the  $n$  medium because of the boundary conditions.

Since the axial dipole is coupled only to the  $z$  component of the vacuum field, which is entirely tangential to the wire surface, the axial dipole will experience the vacuum field strength in the  $n$  medium. In other words, the dipole will radiate as if it were a dipole in the  $n$  medium. As we know, the dipole decay rate is proportional to the factor  $n$ , where  $n$  is the refractive index of the medium surrounding the dipole. This can be seen when Eq. (3.1) is applied to the case of a dielectric medium.<sup>24</sup> Hence, in the limit when  $d_D$  approaches zero, the axial dipole emission rate would be reduced by the factor  $(n/n_D)$  from  $\gamma_\infty$ . The  $n_D$  medium behaves as a bulk medium when the core diameter is large.

The radial dipole, however, has 3/4 of its emission into the TE mode and 1/4 of its emission into the TM mode. Since the TE field is tangential to the wire surface, the radial dipole decay rate that is due to the TE field will be  $3/4(n/n_D)$  of  $\gamma_\infty$ . The TM field component that couples to the radial dipole is perpendicular to the wire surface. Hence its relevant field strength will be reduced by the factor of  $(n/n_D)^2$  from that of the  $n$  medium. Since the decay rate is proportional to the field strength squared, the decay rate of the radial dipole that is due to the TM modes will be reduced by a factor  $(n/n_D)^4$  from its decay rate in the  $n$  medium. But the decay rate in the  $n$  medium is  $(n/n_D)$  of that in a bulk medium of index  $n_D$ . Also when the factor 1/4 is taken into account, the radial dipole decay rate that is due to the TM field should then be  $1/4(n/n_D)^5$  of  $\gamma_\infty$ . Thus we conclude that, when the wire diameter approaches zero, the asymptotic values of the decay rates for the axial dipole  $\gamma_{\text{axial}}$  and radial dipoles  $\gamma_{\text{radial}}$  will be

$$\gamma_{\text{axial}} = (n/n_D)\gamma_\infty, \quad (5.1)$$

$$\gamma_{\text{radial}} = \frac{3}{4}\left(\frac{n}{n_D}\right)\gamma_\infty + \frac{1}{4}\left(\frac{n}{n_D}\right)^5\gamma_\infty. \quad (5.2)$$

This gives us, for the case of  $n = 1$  and  $n_D = 3.4$ ,  $\gamma_{\text{radial}} = 0.22\gamma_\infty$  and  $\gamma_{\text{axial}} = 0.29\gamma_\infty$ , which are in agreement with the values at  $d_D = 0$  in Figs. 3 and 4, respectively. Hence our decay-rate calculations for the radiation modes have the correct values at  $d_D = 0$ .

When the diameter of the wire is large, the contribution to the decay rate that is due to spontaneous emission into the radiation modes  $\gamma_R$  (i.e., those modes that eventually escape from the wire) can be easily computed. In that case we can treat the dipole as emitting into a large dielectric material, and the value of  $\gamma_R$  can be found by integrating over the emission into the shaded region of Fig. 1, defined by the critical angle of escape. In this limit  $\gamma_R$  for the various dipoles emission given by Eq. (3.12) can be simplified to

$$\gamma_R = CR_R, \quad (5.3)$$

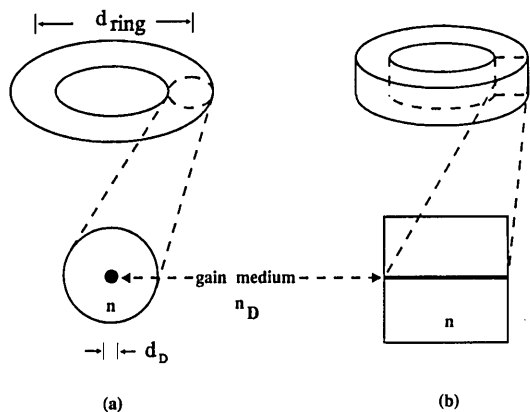


Fig. 6. Schematics of two microcavity ring laser structures. (a) An ideal structure with an active medium along the axis of waveguide. (b) A practical structure with a planar active medium.

where  $C$  is a constant common to all cases and  $R_R$  is given by

$$R_R = \frac{3}{4\pi} \int_0^{2\pi} d\phi \int_{\pi/2-\theta_c}^{\pi/2} d\theta G(\theta, \phi), \quad (5.4)$$

with  $G(\theta, \phi) = (\sin^3 \theta)$  [TM] = 0 [TE] for axial dipole emission into TM and TE modes, and  $G(\theta, \phi) = (\cos^2 \theta) (\sin^2 \phi) (\sin \theta)$  [TM] =  $(\sin^2 \phi) (\sin \theta)$  [TE] for radial dipole emission into TM and TE modes. The critical angle  $\theta_c$  is given by  $\sin \theta_c = (n/n_D)$ . The value of  $C$  is chosen so that  $R_R = 1$  for the total rate of emission from each dipole into all angles and all modes (i.e., the case in which  $\theta_c = \pi/2$ ). For the case in which  $n = 1.0$  and  $n_D = 3.4$ , we have  $R_R = 0.428$  for the total rate of emission of the axial dipole into the TM radiation mode (TE emission is zero). We have  $R_R = 0.227$  for the total rate of emission of the radial dipole into the TM and TE radiation modes (0.0064 into TM, 0.2206 into TE). These are to be compared with the value of  $R_R$  when  $\theta_c = \pi/2$  (i.e., all angles).  $R_R$  is 1 for axial dipole emission into TM modes, 1/4 for radial dipole emission into TM modes, and 3/4 for radial dipole emission into TE modes.

In the limit of a large waveguide diameter, the spontaneous emission will be coupled into many guided modes. The total emission into the guided modes and the radiation modes will approach the bulk value of  $\gamma_\infty$ . That is,  $R_{sp}$  will approach the value of unity, which is already apparent in Figs. 3 and 4.

### 6. CAVITY ENHANCEMENT FACTOR FOR SPONTANEOUS EMISSION

Consider an ideal ring laser, shown in Fig. 6(a), where the ring cavity is formed by a circular ring of cylindrical dielectric waveguide. We assume that the active medium occupies a small region along the center axis of the waveguide. This is similar to the case of the cylindrical waveguide considered above. To calculate the  $\beta$  value, we need to know the fractional power of spontaneous emission into the lasing modes. For the discussion in this section the lasing modes will be taken loosely as the waveguide modes at the spontaneous-emission frequency.

This would be the case for multimode lasing. We specifically consider single-mode lasing in Section 7. If the cavity resonance is weak (i.e., low cavity quality factor  $Q$ ), then the  $\beta$  value for this ring laser can be estimated from Figs. 3 and 4, which give the fraction of spontaneous emission into the waveguide modes. However, with a high- $Q$  cavity, the vacuum-field intensity will be enhanced at the cavity resonant frequencies, which can alter the  $\beta$  value. Thus it is important for us to discuss this cavity-enhancement effect before we present the specific  $\beta$ -value calculations.

The cavity-enhancement effect is dependent on the spectral width of spontaneous emission ( $\Delta\nu_{sp}$ ), the cavity resonance width ( $\Delta\nu_{cav}$ ), and the frequency spacing between two adjacent longitudinal modes ( $\Delta\nu_{mode}$ ). In calculating the  $\beta$  values, it is important to distinguish between the case in which the spectral width of spontaneous emission is smaller than the cavity resonance width ( $\Delta\nu_{sp} < \Delta\nu_{cav}$ ) and the case in which the spectral width of spontaneous emission is larger than the cavity resonance width ( $\Delta\nu_{sp} > \Delta\nu_{cav}$ ). The former case will be referred to as the first case and the latter case will be referred to as the second case. The first case requires a large  $\Delta\nu_{cav}$  and can be achieved with a short cavity. These two cases are illustrated schematically in Fig. 7, where the solid curve is the cold cavity transmission curve, the dashed curve is the spontaneous-emission curve for the first case, and the dotted curve is the spontaneous-emission curve for the second case. In the discussion below, without loss of generality we assume that the spontaneous-emission spectrum is homogeneously broadened. The behavior for the inhomogeneously broadened case can be obtained from the homogeneously broadened case by modeling it as a combination of many homogeneously broadened spectra with different frequency shifts.

For the first case, where  $\Delta\nu_{sp} < \Delta\nu_{cav}$ , the active medium will see a vacuum-field intensity that is strongly modified by the cavity. The frequency dependence of the vacuum-field intensity in the cavity is proportional to the cavity transmission curve. Let us describe the degree of cavity enhancement of the vacuum-field intensity by a

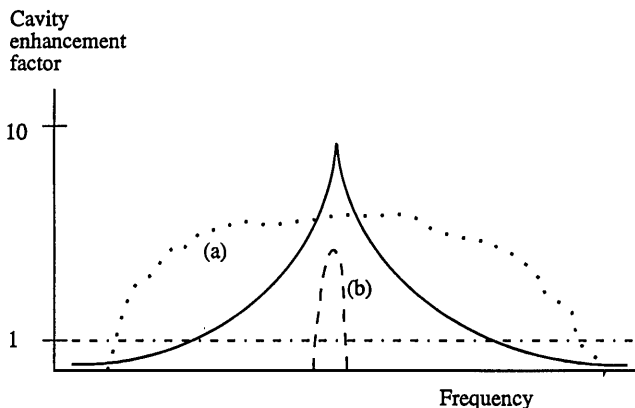


Fig. 7. Cases in which the spontaneous-emission width is (a) larger than and (b) smaller than the cold cavity linewidth. The cavity resonance curve is the solid curve; the spontaneous-emission curves for cases (a) and (b) are the dotted and the dashed curves, respectively. The cavity-enhancement factor that is due to cavity resonance is indicated on the y axis.

cavity-enhancement factor. This enhancement factor is indicated on the  $y$  axis of Fig. 7. In the figure the two-dashed-dotted line represents the unity enhancement factor when there is no cavity effect, and the transmission curve indicates the enhancement factor when there is a cavity effect. For example, if the spontaneous-emission frequency is on resonance with the cavity, and if the cavity has a quality factor of  $Q = 10$ , then the spontaneous-emission rate into the waveguide modes will be increased by a factor of  $\sim 10$  by the cavity. Since the radiation modes will not be affected by the cavity resonance, this means that a larger fraction of spontaneous emission can be channeled into the lasing guided modes. Hence the cavity can be used to drastically increase the value of  $\beta$ .

If most of the emission already goes into the lasing guided modes to start with, then this increase in the value of  $\beta$  will be accompanied by an increase in the total spontaneous-emission rate. The accompanied increase in the total spontaneous-emission rate, however, may not be good for reducing the laser threshold. This is because an increase in the total spontaneous-emission rate would in general increase the transparency pumping rate, which is part of the laser threshold. If the laser threshold is only a few times higher than the transparency pumping rate, then the increase in the transparency pumping rate may balance the beneficial effect of increasing the  $\beta$  value. Hence an overly high cavity-enhancement factor may not be good, and one must be careful to design its value appropriately to optimally reduce the laser threshold.

For the second case, where  $\Delta\nu_{sp} > \Delta\nu_{cav}$ , it can be shown that the spontaneous-emission rate into the guided modes will not be strongly affected by the cavity because the enhancement of the emission rate at cavity resonance is averaged out with the suppression of the emission rate off cavity resonance. Without detailed calculation we can expect that the cavity-enhancement factor will be averaged to near unity if the spontaneous-emission width is nearly the same as or is larger than the frequency spacing between two adjacent longitudinal resonances (i.e.,  $\Delta\nu_{sp} \geq \Delta\nu_{mode}$ ).

## 7. SPONTANEOUS-EMISSION FACTORS FOR MICROCAVITY LASERS

From the discussion in Section 6 we see that, to compute the spontaneous emission factor properly, one has to include both the waveguide effect and the cavity-enhancement factor. However, the cavity-enhancement factor can be computed separately. Hence in the discussion below we consider only the simple case in which the cavity-enhancement factor is unity. As is discussed above, this is the case in which the homogeneously broadened spectral width of the spontaneous emission is nearly the same as or is larger than the cavity intermode frequency spacing. For the discussion in this section we assume that the spontaneous-emission width covers only one cavity resonance. This assumption is necessary in order to optimize the  $\beta$  value for the case of single-mode, single-frequency lasing.

First we calculate the  $\beta$  value for the case of an ideal ring laser, shown in Fig. 6(a). For this calculation we assume that all three dipoles have equal probabilities of being excited. Also, the lasing modes in this ring cavity case will

be taken as the lowest-order guided modes of the waveguide, which are the two orthogonally polarized  $HE_{11}$  modes. In addition, lasing modes in both traveling-mode directions will be included. If we take only one of the polarizations as the lasing mode, then the  $\beta$  value will be effectively halved. If we further take only one of the two traveling-mode directions as the lasing mode, then the  $\beta$  value will be effectively one quarter of the calculated value. However, it is possible to introduce birefringence in the guide to shift the guiding frequency of one of the polarizations off the dipole emission frequency. It is also possible to use active media that have different emission frequencies and efficiencies for different polarizations, such as a transversely placed quantum wire array.<sup>22</sup> This technique would enhance one polarization emission over the other. In addition, it is possible to introduce non-reciprocal elements into the cavity to change the resonance frequency of the lasing modes for different traveling-mode directions. Although they are not easy to realize in practice, these methods may be used to help us to obtain single-mode lasing with a high  $\beta$  value.

Let the diameter of the ring cavity in Fig. 6(a) be  $d_{ring}$  and the diameter of the waveguide be  $d_D$ . The refractive indices of the waveguide ( $n_D$ ) and its surrounding medium ( $n$ ) are assumed to be 3.4 and 1.0, respectively. In order to obtain the largest  $\beta$  value for this ring laser, it is desirable to have as much spontaneous emission into the lasing guided mode as possible. For the purpose of calculating the  $\beta$  value, we assume that the three orthogonal dipoles are equally excited. From Figs. 3 and 4 we see that the largest  $\beta$  value is obtained with  $d_D$  just below the cutoff diameter for the second-lowest-order guided mode (i.e., the  $TM_{01}$  mode). This gives  $d_D = 0.76\lambda/n_D \equiv d_{opt}$ . For a wavelength of  $\lambda = 1 \mu\text{m}$ ,  $d_{opt} = 223.5 \text{ nm}$ . From Fig. 3 we see that the emission from the radial dipoles will be mainly into the  $HE_{11}$  guided mode with a total normalized rate of  $1.2 \times 2 = 2.4$ . (We have included two radial dipoles.) The emission from the two radial dipoles into the radiation modes has a total normalized rate of  $2 \times 0.025 = 0.05$  (Fig. 3). The axial dipole does not emit into any guided modes, and its emission into the radiation modes is suppressed owing to the cavity effect experienced by the radiation modes. (The cavity effect is caused by the waveguide surface.) From Fig. 4 we see that the axial dipole emits only into the radiation modes with a normalized rate of 0.04. Considering all these factors, the  $\beta$  value is then given by  $\beta = 2.4/(2.4 + 0.05 + 0.04) = 0.96$ . We note that this is only the best-case estimate, considering our approximation in the treatment of the radiation modes.

In the worst case, where there is no cavity-suppression effect for the radiation modes, the normalized emission rates into the radiation modes from the dipoles are at most as bad as in the case of the large core diameter limit discussed in Section 5. In that case the total emission rate into the radiation modes from the two radial dipoles and one axial dipole is  $(0.227 \times 2 + 0.428) = 0.882$  [from Eq. (5.4)]. This gives a worst-case  $\beta$  value of  $\beta = 2.4/(2.4 + 0.882) = 0.73$ .

The ideal structure discussed above is not easily realized in practice. A more practical structure is shown in Fig. 6(b), where the waveguide has a rectangular cross section and the active medium is a planar structure such

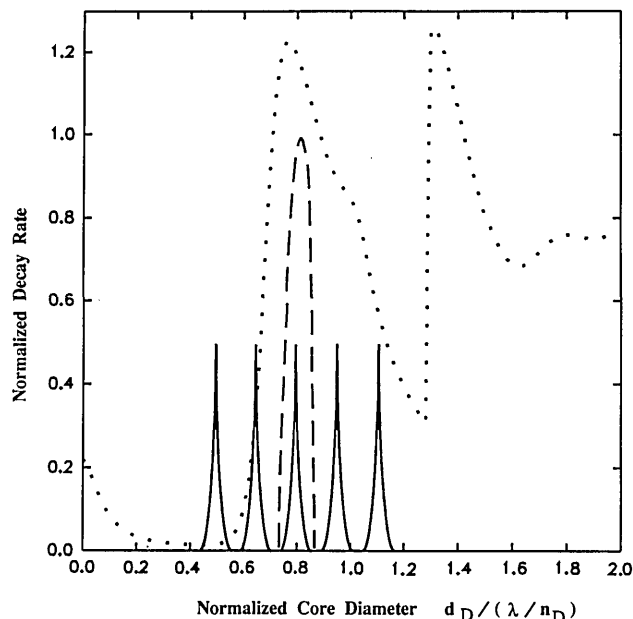


Fig. 8. Cavity resonance (solid curve), free-space spontaneous emission (dashed curve), and decay rate into  $HE_{11}$  mode (dotted curve). The  $x$  axis is read as a function of the frequency proportional to  $n_D/\lambda$ .

as a quantum well. In this structure the main problem is again the lack of resonant suppression for emission into the radiation modes. Furthermore, since the gain medium is not at the waveguide axis, the  $z$  dipole will no longer be prevented from radiating into the lowest-order guided modes. However, this situation will only enhance the emission into the lasing modes and help to increase the  $\beta$  value. Hence we would expect for this structure a maximum  $\beta$  value of better than 0.7, similar to that given by the worst-case situation mentioned above. We can expect this maximum value to be achieved when the waveguide diameter is just below the cutoff diameter for the second guided mode.

It is also of interest to see how large the ring diameter can be before the  $\beta$  value decreases. The resonant frequencies of the ring cavity are given approximately by  $\nu_p = cp/(n_D L)$ , where  $p$  is an integer that indicates the mode number and  $L = \pi d_{\text{ring}}$  is the perimeter of the ring. Since the  $x$  axis of Fig. 3 is  $d_D n_D/\lambda$ , if we keep  $d_D$  fixed then the  $x$  axis can be read as a function of  $n_D/\lambda$  ( $\lambda$  is free-space wavelength), which is proportional to the frequency. As an example, let us assume that the value  $L$  is chosen so that the spontaneous-emission frequency coincides with the peak of the  $HE_{11}$  mode. Let the spontaneous-emission width be  $\Delta\nu_{\text{sp}}$ . We would expect the spontaneous emission to go into one single-cavity resonance mode, provided that  $\Delta\nu_{\text{sp}}$  is smaller than the cavity intermode frequency spacing given by  $\Delta\nu_{\text{mode}} = c/(n_D L)$ . Hence the size of the ring is really determined by  $\Delta\nu_{\text{sp}} < \Delta\nu_{\text{mode}}$ . This relationship is sketched in Fig. 8, where the  $x$  axis is read as a function of the frequency proportional to  $n_D/\lambda$ , the dotted curve is the emission rate into the  $HE_{11}$  mode, the dashed curve is the free-space spontaneous-emission curve, and the solid curve is the cavity resonance curve. A typical spontaneous-emission frequency width from quantum-well excitons is  $\sim 0.01$  of the optical frequency. In that case we can satisfy  $\Delta\nu_{\text{sp}} < \Delta\nu_{\text{mode}}$  with

$L$  as large as  $L = \lambda/(0.01n_D) = 29.4 \mu\text{m}$  (i.e.,  $d_{\text{ring}} = 9.4 \mu\text{m}$ ). In this  $\beta$ -value calculation we have not included the effect of waveguide bending. With our large core-to-cladding refractive-index ratio, this effect is important only when the ring diameter is of the order of an optical wavelength.

To complete the discussion, we reiterate that it is possible further to increase the  $\beta$  values by using a short cavity so that the spontaneous-emission width is smaller than the cold cavity transmission width. However, as is pointed out in Section 6, the cavity must be carefully designed to yield a beneficial reduction in the laser threshold. This is especially so if the waveguide effect already gives a reasonably high  $\beta$  value.

Our analysis can also be applied to the laser structure shown in Fig. 9, where the laser cavity is simply a vertical cylindrical dielectric waveguide with high-reflection-coated end facets. The active medium can be a quantum well between the two mirrors, placed at the enhanced region of the cavity standing-wave field. This is similar to the structure of some currently fabricated vertical-cavity surface-emitting lasers.<sup>26</sup> This case is basically no different from the ring-cavity case without resonant suppression for the radiation modes. We conclude that, when the waveguide diameter is near 223.5 nm, the  $\beta$  value for this structure should also be near 0.7 (with a unity cavity-enhancement factor). Similarly, if the spontaneous-emission width is 1% of the optical frequency, then the length of the cavity can be as long as  $100\lambda/n_D$  without affecting the  $\beta$  value. This is a great advantage over the nonguided vertical-cavity structure, for which a microcavity effect can be achieved only if the length of the cavity is of the order of one wavelength. In this simple estimation we have not included additional enhancement of the emission into the lasing mode when the active medium is placed at an antinode of the cavity standing-wave field.

## 8. CONCLUSION

We have studied the modification of spontaneous emission from excitons in a cylindrical dielectric waveguide. The waveguide is assumed to have a high reflective index of 3.4, which is typical for most semiconductor materials. The excited dipoles that represent the excitons are assumed to be situated along the axis of the waveguide. From the study we conclude that with an appropriately chosen waveguide diameter a substantial amount of spontaneous emission can be channeled into the two orthogonally po-

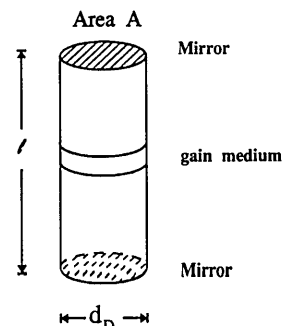


Fig. 9. Vertical-cavity surface-emitting laser with vertical waveguiding through a cylindrical waveguide structure.

larized lowest-order guided modes. The waveguide is then joined end to end to form an ideal ring laser cavity, for which we show that a  $\beta$  value of  $\sim 0.96$  can be achieved. Our study shows that to achieve this optimal  $\beta$  value the waveguide diameter should be just below the cutoff diameter for the second-lowest-order guided mode (near 220.0 nm) at a 1- $\mu\text{m}$  wavelength). We then consider a more easily realized ring laser cavity structure. We show that the  $\beta$  value for this structure still can be near 0.7. The analysis is then applied to estimate the  $\beta$  value of a vertical-cavity laser with vertical waveguiding. Again, a  $\beta$  value of better than 0.7 is estimated.

In our analysis we show that the high  $\beta$  value can be obtained even when the effective cavity length of the ring laser or vertical-cavity laser is much longer than an optical wavelength. This result is due to the one-dimensional nature of the cavities. In conclusion, microlasers based on strongly guided single-mode dielectric waveguides are promising for achieving high  $\beta$  values and low lasing thresholds.

## Appendix A

In this appendix we show some examples of the mode functions  $F_m(r, \phi)$  that are used for calculating the rate of spontaneous emission into the guided modes,  $r_g$ . Since the structure of the dielectric waveguide under consideration is a step-index cylindrical waveguide, all the field components of the guided modes throughout the structure can be solved by means of the wave equation in the cylindrical coordinates.<sup>27</sup> The field vector  $\mathbf{F}_m(r, \phi)$  can be expressed in terms of the coordinates as

$$\mathbf{F}_m(r, \phi, z) = F_r \hat{r} + F_\phi \hat{\phi} + F_z \hat{z}. \quad (\text{A1})$$

In the core region  $n_D$ ,  $F_r$ ,  $F_\phi$ , and  $F_z$  are given by

$$F_r = \left[ \frac{-ik_{mz}}{h} A J_l'(hr) + \frac{\omega\mu l}{h^2 r} B J_l(hr) \right] \exp(i\eta), \quad (\text{A2})$$

$$F_\phi = \left[ \frac{lk_{mz}}{h^2 r} A J_l(hr) + \frac{i\omega\mu}{h} B J_l'(hr) \right] \exp(i\eta), \quad (\text{A3})$$

$$F_z = A J_l(hr) \exp(i\eta), \quad (\text{A4})$$

whereas in the cladding region of index  $n$  they are given by

$$F_r = \left[ \frac{ik_{mz}}{q} C K_l'(qr) - \frac{\omega\mu l}{q^2 r} D K_l(hr) \right] \exp(i\eta), \quad (\text{A5})$$

$$F_\phi = \left[ -\frac{lk_{mz}}{q^2 r} C K_l(qr) - \frac{i\omega\mu}{q} D K_l'(qr) \right] \exp(i\eta), \quad (\text{A6})$$

$$F_z = C K_l(qr) \exp(i\eta), \quad (\text{A7})$$

where  $\eta = \omega t + l\phi - k_{mz}z$ .  $J_l$  is the Bessel function of the first kind of order  $l$ , and  $K_l$  is the modified Bessel function of the second kind of order  $l$ .  $k_{mz}$  is the propagation constant of the guided mode. Also,  $h^2 = k^2 - k_{mz}^2$  and  $q^2 = k_{mz}^2 - k^2$  determine the values of  $h$  and  $q$ . The field components must satisfy the boundary conditions, which in turn determine the propagation constant  $k_{mz}$ . The ratios between four constants,  $A$ ,  $B$ ,  $C$ , and  $D$ , can be obtained from the boundary condition that  $F_\phi$  and  $E_z$  be continuous at the core-to-cladding interface. These ra-

tios are given by

$$\frac{C}{A} = \frac{J_l(ha)}{K_l(qa)}, \quad (\text{A8})$$

$$\frac{B}{A} = \frac{ik_{mz}l}{\omega\mu} \left( \frac{1}{q^2 a^2} + \frac{1}{h^2 a^2} \right) \left( \frac{J_l'(ha)}{ha J_l(ha)} + \frac{K_l'(qa)}{qa K_l(qa)} \right)^{-1}, \quad (\text{A9})$$

$$\frac{D}{A} = \frac{J_l(ha)}{K_l(qa)} \frac{B}{A}. \quad (\text{A10})$$

The value of the propagation constant  $k_{mz}$  for each guided mode can be found from the following mode equations:

HE mode,

$$\frac{J_{l-1}(ha)}{ha J_l(ha)} = -\frac{n_D^2 + n^2}{2n_D^2} \frac{K_l'(qa)}{qa K_l(qa)} + \left[ \frac{l}{(ha)^2} + R \right]; \quad (\text{A11})$$

EH mode,

$$\frac{J_{l+1}(ha)}{ha J_l(ha)} = \frac{n_D^2 + n^2}{2n_D^2} \frac{K_l'(qa)}{qa K_l(qa)} + \left[ \frac{l}{(ha)^2} - R \right]; \quad (\text{A12})$$

TE mode,

$$\frac{J_1(ha)}{ha J_0(ha)} = -\frac{K_1(qa)}{qa K_0(qa)}; \quad (\text{A13})$$

TM mode,

$$\frac{J_1(ha)}{ha J_0(ha)} = \frac{n^2 K_1(qa)}{qa n_D^2 K_0(qa)}. \quad (\text{A14})$$

The variable  $R$  in Eqs. (A11) and (A12) is given by

$$R = \left\{ \left( \frac{n_D^2 - n^2}{2n_D^2} \right)^2 \left[ \frac{K_l'(qa)}{qa K_l(qa)} \right]^2 + \left( \frac{lk_{mz}}{n_D k_0} \right)^2 \left( \frac{1}{q^2 a^2} + \frac{1}{h^2 a^2} \right)^2 \right\}^{1/2}. \quad (\text{A15})$$

These mode equations can be solved graphically and numerically. The eigenvalue solutions, i.e.,  $k_{mz}$  for different radii of the core  $n_D$ , are essential for obtaining the field components and the decay rates of each mode. The modes of main interest to us are those modes with  $l = 0$  and  $l = \pm 1$ . Those modes with  $l = 0$  are linearly polarized, and their coupling to the dipoles can be easily obtained. Those modes with  $l = \pm 1$ , such as the hybrid modes, can be made into linearly polarized modes by means of linear combinations of the  $l = 1$  and  $l = -1$  mode functions.

## REFERENCES

1. F. De Martini and G. R. Jacobovitz, "Anomalous spontaneous-stimulated-decay phase transition and zero-threshold laser action in a microscopic cavity," *Phys. Rev. Lett.* **60**, 1711-1714 (1988).
2. E. Yablonovitch, "Inhibited spontaneous emission in solid-state physics and electronics," *Phys. Rev. Lett.* **58**, 2059-2062 (1987).
3. G. Bjork and Y. Yamamoto, "Analysis of semiconductor micro-cavity lasers using rate equations," *IEEE J. Quantum Electron.* **27**, 2386-2396 (1991).
4. R. G. Hulet, E. S. Hilfer, and D. Kleppner, "Inhibited sponta-

- neous emission by a Rydberg atom," *Phys. Rev. Lett.* **55**, 2137–2140 (1985).
5. F. De Martini, G. Innocenti, G. R. Jacobovitz, and P. Mataloni, "Anomalous spontaneous emission time in a microscopic optical cavity," *Phys. Rev. Lett.* **59**, 2955–2958 (1987).
  6. J. Martorell and N. M. Lawandy, "Observation of inhibited spontaneous emission in a periodic dielectric structure," *Phys. Rev. Lett.* **65**, 1877–1880 (1990).
  7. J. Martorell and N. M. Lawandy, "Spontaneous emission in a disordered dielectric medium," *Phys. Rev. Lett.* **66**, 887–890 (1991).
  8. A. J. Campillo, J. D. Eversole, and H.-B. Lin, "Cavity quantum electrodynamic enhancement of stimulated emission in microdroplets," *Phys. Rev. Lett.* **67**, 437–440 (1991).
  9. G. Bjork, S. Machida, Y. Yamamoto, and K. Igeta, "Modification of spontaneous emission rate in planar dielectric microcavity structures," *Phys. Rev. A* **44**, 669–681 (1991).
  10. M. Suzuki, H. Yokoyama, S. D. Brorson, and E. P. Ippen, "Observation of spontaneous emission lifetime change of dye-containing Langmuir–Blodgett films in optical microcavities," *Appl. Phys. Lett.* **58**, 998–1000 (1991).
  11. H. Yokoyama, K. Nishi, T. Anan, H. Yamada, S. D. Brorson, and E. P. Ippen, "Enhanced spontaneous emission from GaAs quantum wells in monolithic microcavities," *Appl. Phys. Lett.* **57**, 2814–2816 (1990).
  12. H. Yokoyama, M. Suzuki, and Y. Nambu, "Spontaneous emission and laser oscillation properties of microcavities containing a dye solution," *Appl. Phys. Lett.* **58**, 2598–2600 (1991).
  13. S. D. Brorson, H. Yokoyama, and E. P. Ippen, "Spontaneous emission rate alteration in optical waveguide structures," *IEEE J. Quantum Electron.* **26**, 9, 1492–1499 (1990).
  14. D. G. Deppe and C. Lei, "Spontaneous emission from a dipole in a semiconductor microcavity," *J. Appl. Phys.* **70**, 3443–3448 (1991).
  15. K. A. Shore, "Control of spontaneous emission in microcavity laser-diodes," *Physica B* **175**, 123–126 (1991).
  16. S. T. Ho, S. L. McCall, R. E. Slusher, L. N. Pfeiffer, K. W. West, A. F. J. Levi, G. E. Blonder, and J. L. Jewel, "High index contrast mirrors for optical microcavities," *Appl. Phys. Lett.* **57**, 1387–1389 (1990).
  17. R. E. Slusher, S. L. McCall, J. B. Stark, A. F. J. Levi, R. A. Logan, and S. J. Pearton, "Semiconductor microdisk lasers," in *Annual Meeting, 1991 OSA Technical Digest Series* (Optical Society of America, Washington, D.C., 1991), postdeadline papers, p. 27.
  18. T. Kobayashi, T. Segawa, A. Morimoto, and T. Sueta, "Novel-type lasers, emitting devices, and functional optical devices by controlling spontaneous emission," presented at the 46th Fall Meeting of the Japanese Applied Physics Society, 1982.
  19. E. Yablonovitch and T. J. Gmitter, "Photonic band structure: the face-centered cubic case," *Phys. Rev. Lett.* **63**, 1950–1953 (1989).
  20. Y. Suematsu and K. Furuya, "Theoretical spontaneous emission factor of injection lasers," *Trans. Inst. Electron. Commun. Eng.* **60**, 467–472 (1977).
  21. H. Yokoyama and S. D. Brorson, "Rate equation analysis of microcavity lasers," *J. Appl. Phys.* **66**, 4801–4805 (1989).
  22. T. Baba, T. Hamano, F. Koyama, and K. Iga, "Spontaneous emission factor of a microcavity DBR surface-emitting laser," *IEEE J. Quantum Electron.* **27**, 1347–1358 (1991).
  23. Y. Yamamoto, S. Machida, and G. Bjork, "Microcavity semiconductor laser with enhanced spontaneous emission," *Phys. Rev. A* **44**, 657–668 (1991).
  24. D. Marcuse, *Principles of Quantum Electronics* (Academic, New York, 1980).
  25. G. Bjork and O. Nilsson, "A new exact and efficient numerical matrix theory of complicated laser structure: properties of asymmetric phase-shifted DFB lasers," *IEEE J. Lightwave Technol.* **LT-5**, 140–146 (1987).
  26. J. L. Jewell, J. P. Harbison, A. Scherer, Y. H. Lee, and L. T. Florez, "Vertical-cavity surface-emitting lasers: design, growth, fabrication, characterization," *IEEE J. Quantum Electron.* **27**, 1332–1346 (1991).
  27. A. Yariv, *Optical Electronics*, 4th ed. (Holt, Rinehart & Winston, New York, 1985).